ACS NANO
Cite This: ACS Nano XXXX, XXX, XXX−XXX
www.acsnano.org

ARTICLE

Electronic Properties of Transferable Atomically Thin $MoSe_2$/h-BN Heterostructures Grown on Rh(111)

Ming-Wei Chen,[†,‡] HoKwon Kim,[†,‡] Carlo Bernard,[§] Michele Pizzochero,[∥] Javier Zaldívar,[⊥] Jose Ignacio Pascual,[⊥,#] Miguel M. Ugeda,[#,¶,∞] Oleg V. Yazyev,[∥] Thomas Greber,[§] Jürg Osterwalder,[§] Olivier Renault,[△,▲] and Andras Kis[*,†,‡]

[†]Electrical Engineering Institute, [‡]Institute of Materials Science and Engineering, and [∥]Institute of Physics, École Polytechnique Fédérale de Lausanne (EPFL), CH-1015 Lausanne, Switzerland

[§]Physik-Institut, University of Zurich, 8057 Zurich, Switzerland

[⊥]CIC nanoGUNE, 20018 Donostia-San Sebastian, Spain

[#]Ikerbasque, Basque Foundation for Science, 48013 Bilbao, Spain

[¶]Donostia International Physics Center (DIPC), Manuel Lardizábal 4, 20018 San Sebastián, Spain

[∞]Centro de Física de Materiales (CSIC-UPV/EHU), Manuel Lardizábal 5, 20018 San Sebastián, Spain

[△]Université Grenoble Alpes, F-38000 Grenoble, France

[▲]CEA, LETI, MINATEC Campus, F-38054 Grenoble, France

Supporting Information

Downloaded via ECOLE POLYTECHNIC FED LAUSANNE on November 2, 2018 at 22:03:43 (UTC).
See https://pubs.acs.org/sharingguidelines for options on how to legitimately share published articles.

ABSTRACT: Vertically stacked two-dimensional (2D) heterostructures composed of 2D semiconductors have attracted great attention. Most of these include hexagonal boron nitride (h-BN) as either a substrate, an encapsulant, or a tunnel barrier. However, reliable synthesis of large-area and epitaxial 2D heterostructures incorporating BN remains challenging. Here, we demonstrate the epitaxial growth of nominal monolayer (ML) $MoSe_2$ on h-BN/Rh(111) by molecular beam epitaxy, where the $MoSe_2$/h-BN layer system can be transferred from the growth substrate onto SiO_2. The valence band structure of ML $MoSe_2$/h-BN/Rh(111) revealed by photoemission electron momentum microscopy (*k*PEEM) shows that the valence band maximum located at the *K* point is 1.33 eV below the Fermi level (E_F), whereas the energy difference between *K* and Γ points is determined to be 0.23 eV, demonstrating that the electronic properties, such as the direct band gap and the effective mass of ML $MoSe_2$, are well preserved in $MoSe_2$/h-BN heterostructures.

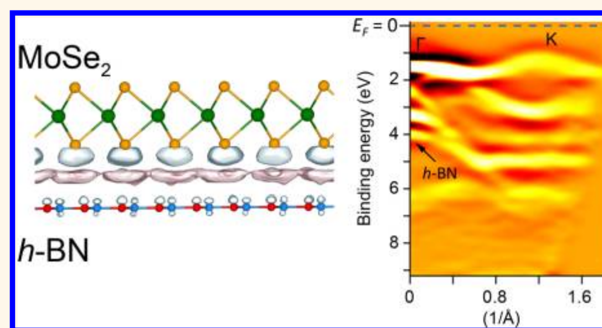

KEYWORDS: *two-dimensional materials, two-dimensional semiconductors, $MoSe_2$, epitaxial growth, h-BN substrates*

Distinct electronic[1] and optical properties[2,3] make atomically thin two-dimensional materials and transition metal dichalcogenides (TMDs)[4,5] attractive for fundamental research and practical applications. The lack of dangling bonds at their surface makes integration into van der Waals (vdW) heterostructures[6] possible, further extending their reach.

Most of the vdW heterostructures being studied today incorporate hexagonal boron nitride (h-BN) as a substrate[7,8] and encapsulation layer, where the atomically flat surface of h-BN crystals and the low defect density allow the intrinsic properties of 2D materials to be accessed. Moreover, the wide band gap of h-BN in the UV range makes it promising as a tunnel barrier, whereas its dielectric properties also allow it to sustain high electric fields before breakdown.[9] However, the reliable preparation of large-area heterostructures remains challenging. The common approach consists of preparing them by mechanical exfoliation and transfer processes, which can introduce residues and contaminants at the interface while the process itself is not scalable.

Chemical vapor deposition (CVD) has been proposed for growing various 2D materials with good quality, but the use of

Received: July 25, 2018
Accepted: October 25, 2018
Published: October 29, 2018

 © XXXX American Chemical Society

DOI: 10.1021/acsnano.8b05628
ACS Nano XXXX, XXX, XXX−XXX

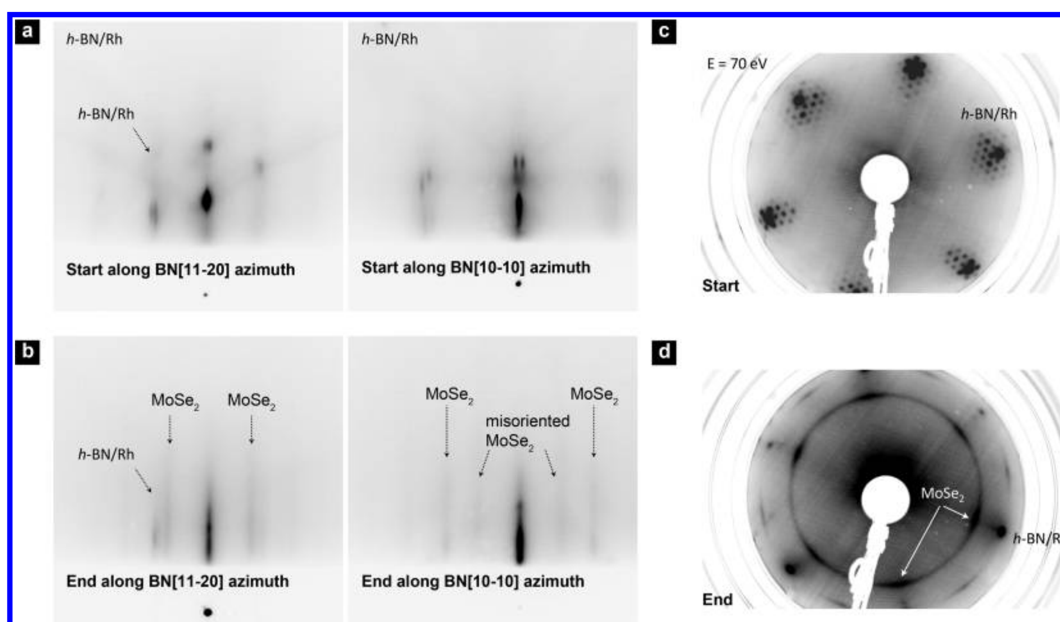

Figure 1. Growth of atomically thin $MoSe_2$/h-BN heterostructures. (a,b) *In situ* RHEED observation during growth along h-BN [11−20] and [10−10] azimuths, respectively. $MoSe_2$ streaks are indicated by black arrows. (c,d) LEED observation of pristine h-BN/Rh(111) (c) and the as-grown $MoSe_2$/h-BN/Rh(111) heterostructure (d).

various precursors for different material systems may increase complexity.[10−13] However, molecular beam epitaxy (MBE) can provide a promising alternative route and exhibits several potential advantages including the use of an ultrahigh vacuum (UHV) environment, high-purity sources, and the capability for *in situ* growth monitoring using reflection high-energy electron diffraction (RHEED). The concept of vdW epitaxy was first proposed by Koma *et al.* in the 1990s, and a wide variety of 2D materials have been studied since then.[6,14−17] However, the MBE growth of 2D vdW heterostructures such as $MoSe_2$/h-BN[15] needs further study, and methods for transferring the resulting heterostack from the metallic substrate also need to be developed.

Here, both the h-BN substrate and the two-dimensional semiconductor $MoSe_2$ are synthesized using scalable methods. We benefit from the previous development of the synthesis of large-scale monolayer (ML) h-BN nanomesh on Rh(111)[18−20] and demonstrate the growth of atomically thin $MoSe_2$ on ML h-BN/Rh(111) substrates by MBE. There were no intermediate chemical states detected in the X-ray photoelectron spectroscopy (XPS) resulting from hybridization. Surprisingly, the 3D nanomesh morphology of BN disappears during $MoSe_2$ growth, resulting in an atomically flat surface over the length of the substrate, with each layer preserving its lattice constant, in contrast with a previous work on $MoSe_2$/h-BN/Ru(0001) systems.[15] We have also succeeded in transferring the resulting stacks onto insulating substrates. The ML $MoSe_2$/h-BN heterostructure after transfer shows photoluminescence (PL) with the main peak at 1.57 eV at room temperature. We further reveal the electronic properties of ML $MoSe_2$/h-BN heterostructures by photoemission electron momentum microscopy (*k*PEEM) and perform density functional theory (DFT) calculations to understand the observed effects.

RESULTS

Growth of Atomically Thin $MoSe_2$/h-BN Heterostructures. Wafer-scale monolayer h-BN featuring a nanomesh structure was grown on Rh(111) using CVD in a UHV environment.[18,19] The h-BN/Rh(111) wafer was cut into 1 × 1 cm^2 pieces and transferred into a separate MBE system. The growth of $MoSe_2$ was monitored *in situ* using RHEED. At the growth start, the streaks from epitaxial h-BN/Rh(111) were observed along two different azimuths, [10−10] and [11−20], respectively (Figure 1a,b). Satellite patterns representing the nanomesh structures of h-BN/Rh(111) can be observed on top of the (00) specular streak. During growth, $MoSe_2$ streaks emerge and remain unchanged until the end of the growth. We estimate that the growth time for a complete monolayer is ∼30 min. At this point, we can observe both streaks from the substrate and $MoSe_2$ along the [11−20] azimuth. The streak spacing indicates that the as-grown $MoSe_2$ film retains the crystal lattice registry without showing detectable strain from the substrate, as expected from vdW epitaxy. This finding is also consistent with results obtained from scanning tunneling microscopy, showing that the as-grown epitaxial $MoSe_2$ films were modulated by the underlying h-BN while the lattice constants for each layer were preserved (Supporting Information section 1). On the other hand, we noticed that in addition to the main $MoSe_2$ streaks shown along the [10−10] azimuth, additional faint streaks also appeared between the main streaks. These could be attributed to the misoriented $MoSe_2$ domains.

We have further examined pristine h-BN and as-grown heterostructures using low-energy electron diffraction (LEED). We can clearly observe a transition from the six-fold superstructure spots related to the h-BN/Rh(111) nanomesh (Figure 1c) to six smeared spots. An aligned six-fold pattern with a larger lattice constant has also appeared, corresponding to the formation of epitaxial $MoSe_2$, whereas the ring pattern in Figure 1d indicates the presence of misoriented domains, in line with RHEED observations. From the LEED intensity distribution analysis, the fraction of aligned $MoSe_2$ can be estimated to be about 42% (Supporting Information section 2). Both $MoSe_2$ and h-BN have preserved their pristine lattices,

DOI: 10.1021/acsnano.8b05628
ACS Nano XXXX, XXX, XXX−XXX

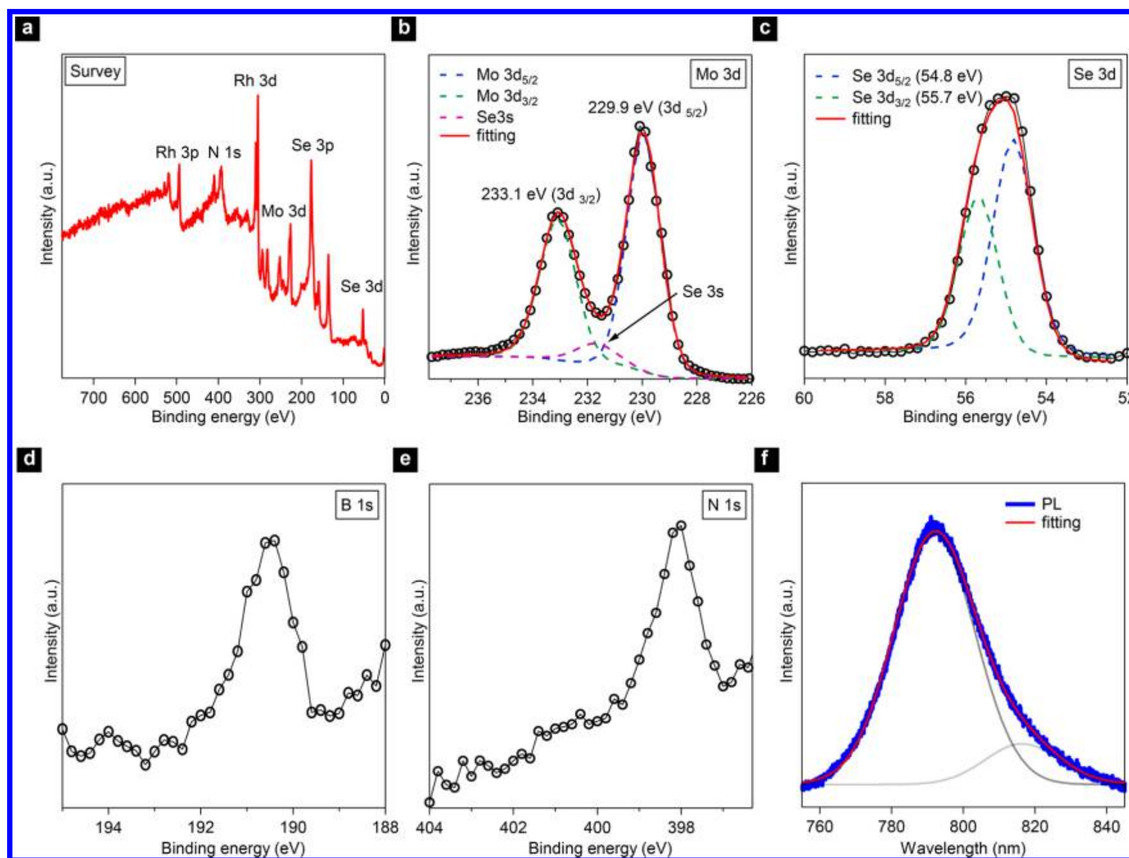

Figure 2. XPS analysis of the $MoSe_2$/h-BN heterostructure. (a) Survey spectrum of the heterostructure. Core-level spectra of (b) Mo 3d, (c) Se 3d, (d) B 1s, and (e) N 1s. (f) Room-temperature PL of the heterostructure transferred onto SiO_2/Si and the fitting (red line) with the deconvolution into two peaks.

although the lattice mismatch is as large as ∼32% considering epitaxy in the (111) planes.

Spectroscopic Analysis of $MoSe_2$/h-BN Heterostructures. The XPS survey of as-grown $MoSe_2$/h-BN/Rh(111) is shown in Figure 2a. The spectrum exhibits a rich feature from both the Rh substrate and the $MoSe_2$/h-BN heterostructure. The Mo $3d_{3/2}$ and Se $3d_{3/2}$ core-level spectra shown in Figure 2b,c, respectively, exhibit characteristic binding energies of 233.1 and 55.7 eV, with the stoichiometric analysis indicating a Se-deficient film (Supporting Information section 3).[14,21] In the Mo 3d core-level region, the Se 3s core-level peak at 231.7 eV overlaps with the Mo 3d peaks, making precise quantification a challenge. Nevertheless, the two featured peak positions related to Mo $3d_{3/2}$ and Mo $3d_{5/2}$ can be easily distinguished, with very little or no trace of oxidation on the high binding energy side.[14] In the Se 3d core level, the binding energy splitting due to spin−orbit coupling can also be deconvoluted, as shown in fits on Figure 2c. The results imply that only Mo−Se covalent bonding exists without a detectable trace of intermediate compounds or oxidation at the interface. Although the signals were mainly from the top layer of $MoSe_2$ and the thicker substrate, we have still observed weak signals corresponding to B 1s and N 1s levels located at binding energies of 190.5 and 398.0 eV, respectively. In another sample with the growth time of 60 min, we estimated the stoichiometry by integrating the peak area and found that the $MoSe_2$ film was Se-deficient, with a thickness corresponding to a nominal bilayer, which is consistent with the estimation from RHEED pattern transition (Supporting Information section 3).

Photoluminescence spectroscopy was first performed on as-grown heterostructures at room temperature. No detectable PL signal was seen due to the quenching effect from the metal substrate.[14,15,22] We have therefore adapted an electrochemical delamination process to transfer the as-grown heterostructure onto fresh SiO_2/Si chips.[23−28] Raman spectra of as-grown and transferred $MoSe_2$/h-BN are comparable and show A_{1g} modes of $MoSe_2$ at ∼240 cm^{-1} (Supporting Information note 4). The PL spectrum acquired from the transferred ML $MoSe_2$/h-BN heterostructure at room temperature is shown in Figure 2f. The asymmetric spectrum is deconvoluted into two parts. The sharp main peak is located at 792 nm (∼1.57 eV) with a line width of 50 meV, whereas a broad sideband is found at 816 nm (∼1.52 eV). The sideband on the low-energy side can be attributed to emission from defect-bound excitons[29] and possibly originates from the local inhomogeneity of the nominal ML which can broaden the main peak on the low-energy side.[30] On the other hand, the sharp main peak at 1.57 eV at room temperature is consistent with reported values for ML $MoSe_2$,[29−32] indicating that the PL of transferred ML $MoSe_2$ is not affected by the underlying h-BN, as expected, and that it can be quenched by the Rh substrate. Considering that the emission from trions is supposed to disappear at room temperature due to thermal fluctuations, the emission should be mainly from the neutral excitons.[32] These results demonstrate the good optical properties of the ML $MoSe_2$/h-BN heterostructure.

Photoemission Electron Momentum Microscopy of the ML $MoSe_2$/h-BN Heterostructures. We have performed *k*PEEM to further investigate the electronic properties

DOI: 10.1021/acsnano.8b05628
ACS Nano XXXX, XXX, XXX−XXX

of as-grown ML $MoSe_2$/h-BN heterostructures. Unlike conventional angle-resolved photoelectron spectroscopy, which requires a predefined high-symmetry direction and is usually time-consuming due to the sequential acquisition of the *k*-space photoemission signal by sample rotation, *k*PEEM uses parallel angular detection at a given photoelectron energy in the valence band by spectroscopic imaging of the back focal plane of the PEEM. Therefore, the entire reciprocal space is sampled, which makes *k*PEEM an ideal tool for directly assessing the electronic properties of 2D materials.[33,34] The three-dimensional imaging not only provides the band structures along high symmetry points but also gives insights into the film quality and band distortion due to interaction with the substrate.[34,35] Here, *k*PEEM was performed with *off*-normal vacuum ultraviolet excitation (He I, $h\nu$ = 21.2 eV), providing an enhanced transition probability at the Γ point,[33,34] thereby facilitating the determination of the valence band maximum (VBM).[36]

Representative images of the *k*PEEM spectroscopic image series of the heterostructure are shown in Figure 3. The signal

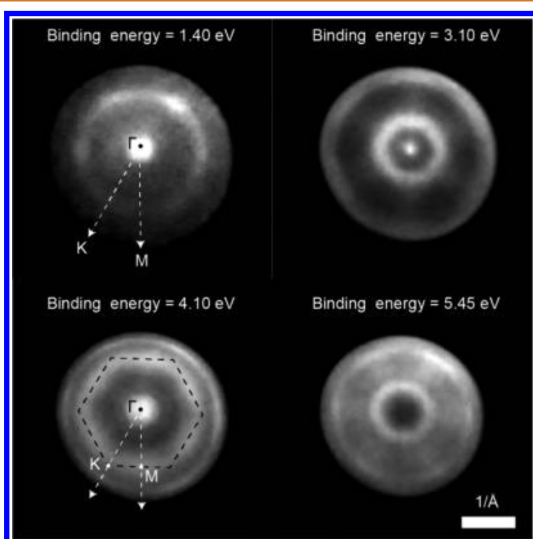

Figure 3. Imaging of heterostructures in *k*-space by *k*PEEM. Images were acquired at different binding energy levels, and the six-fold symmetry is highlighted depicting the first surface Brillouin zone. The high symmetry points Γ, *K*, and *M* of the dominant $MoSe_2$ lattice in *k*-space are shown.

originates from a selected area in real space defined by a field aperture of ~20 μm diameter, containing mostly monolayer crystals with a fraction of bilayer areas, corresponding to a diameter of ~2 $Å^{-1}$ in reciprocal space, thereby sampling the whole first surface Brillouin zone. In the set of *k*PEEM images, the six-fold symmetry of the bands is clearly revealed, indicating the preferred epitaxial directions of $MoSe_2$. In the image at an energy of 4.10 eV in Figure 3, the first surface Brillouin zone and the characteristic high-symmetry points Γ, *K*, and *M* are depicted. We note that the bright spot at the Γ point at the binding energy of 3.1 eV is related to the underlying h-BN, which will be discussed later. In the image stack, we can then perform a cut along the high-symmetry direction Γ to *K* in the binding energy range down to 9.2 eV with respect to E_F = 0 eV, allowing us to obtain the full valence band structure of $MoSe_2$/h-BN.

DISCUSSION

Electronic Properties of the $MoSe_2$/h-BN Heterostructures. To gain an insight into the valence band structure of $MoSe_2$/h-BN, we have first calculated the band structure of free-standing ML $MoSe_2$ by DFT (Figure 4a). Except for the doublet splitting of the valence band induced by spin−orbit coupling, the most significant feature of ML $MoSe_2$ that emerges is the direct band gap where the VBM is at the *K* point, while the Γ point is located 0.23 eV below the VBM. The full valence band structure of nominal ML $MoSe_2$/h-BN/Rh(111) along Γ to *K*, derived from the *k*PEEM image series, is shown in Figure 4b. We have further calculated the second derivative of the *k*PEEM images to enhance the contrast and visibility, especially in the upper valence band region (Figure 4c). In the $MoSe_2$/h-BN heterostructure, the h-BN bands coexist with $MoSe_2$ bands. The σ-band of h-BN originating at a binding energy of 4.0 eV at the Γ point can be identified in Figure 4b,c, as the calculated $MoSe_2$ bands in Figure 4a indicate the absence of band features from $MoSe_2$ there. The result is in line with the *k*PEEM image at an energy of 4.1 eV shown in Figure 3. The π-band of h-BN, which is expected to disperse from the energy of 8.4 eV at Γ point and up to the energy of 2.4 eV at *K* point, is hardly distinguishable as it is masked by the $MoSe_2$ band structure. In the submonolayer $MoSe_2$/h-BN sample, however, the band structure of h-BN is much more clearly resolved (Supporting Information section 5). This observation of a close-to-ideal h-BN band structure is in contrast with the electronic band structure of the h-BN nanomesh on Rh or Ru, where split bands can be observed because of the differences in the interfacial distances between the "pore" and "wire" regions of the nanomesh.[37] Overall, the valence band structure of $MoSe_2$/h-BN resembles those of the free-standing counterpart, without any evidence of interlayer hybridization.

We now focus on the upper valence band dispersions of the $MoSe_2$/h-BN heterostructure in the momentum space along the Γ to *K* direction. First, we do not observe the spin-splitting but a broad band at the *K* point, likely due to the limited energy resolution (100 meV) provided by the microscope settings used in the experiment as well as the contribution from the misoriented domains. The *K* point at a binding energy of 1.33 eV below E_F indicates that the as-grown $MoSe_2$ is unintentionally n-doped, as observed for a majority of reported $MoSe_2$ atomically thin films.

Only one band at an energy of ~1.56 eV at the Γ point is observed, thus indicating that the signal is mainly from the top ML $MoSe_2$ and that the band features of h-BN are absent in the upper valence band structure. Additionally, we compare the band maximum at Γ and *K* points and observe that the VBM located at the *K* point is higher than that of the Γ point by 0.23 eV (Supporting Information section 6). While this value matches our PBE-DFT calculations for free-standing $MoSe_2$ within the range of error, it is lower than the previously reported value of 0.38 eV for ML $MoSe_2$ grown on bilayer graphene on SiC.[31] This could be due to the use of different substrates and a lower measurement resolution in our case.

The direct band gap feature of ML $MoSe_2$ is thus preserved in the heterostructure, and the valence band structure is similar to the calculations for free-standing ML $MoSe_2$. The close examination of the experimental and theoretical band structures reveals the presence of a small band compression, often associated with the presence of a substrate.[34,35,38]

DOI: 10.1021/acsnano.8b05628
ACS Nano XXXX, XXX, XXX−XXX

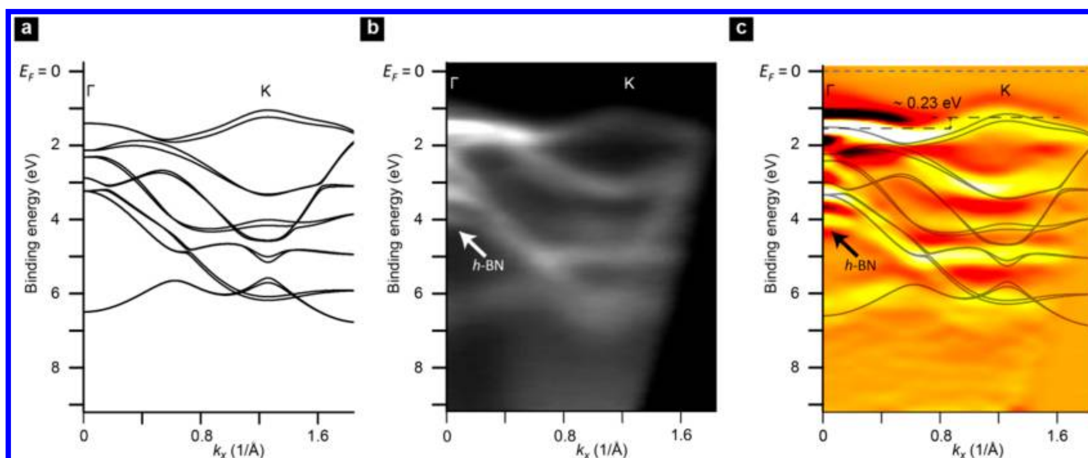

Figure 4. Electronic structure of nominal ML $MoSe_2$/h-BN. (a) Calculated band structures of free-standing ML $MoSe_2$. (b) Reslice of *k*-space along the Γ−*K* direction and (c) the second-derivative of the band structure for enhanced contrast. The calculated structures (black lines) are shown in comparison, and the band maximums at Γ and *K* with the energy difference are specified. The blue dashed line in (c) refers to E_F = 0 eV.

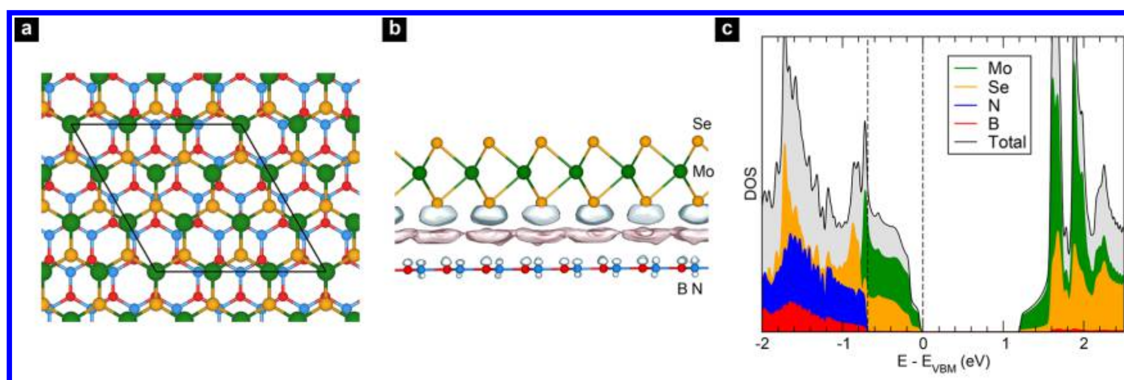

Figure 5. DFT calculations of the $MoSe_2$/h-BN heterostructure. (a) Top view of the model adopted in our vdW-DFT simulations; green, orange, red, and blue balls represent Mo, Se, B, and N atoms, respectively. (b) Difference in charge density between the heterostructure and isolated $MoSe_2$ and h-BN MLs as obtained with the DRSLL functional; gray (pink) clouds indicate negative (positive) charge, and isosurfaces were set to 0.003 e/Å^3. (c) Electronic density of states of the $MoSe_2$/h-BN heterostructure, as obtained with the DRSLL functional; B and N states are doubled to guide the eye, and vertical black dashed lines indicate $MoSe_2$ and h-BN valence band edges.

Similarly, the band dispersions along Γ to *M* are also plotted, and the band structures are in line with the theoretical calculations, with the exception of an energy upshift near the *M* point (Supporting Information section 7). Although the differences are small in our case, this is possibly due to screening by the substrate and charge redistribution at the interface caused by the metallic Rh substrate below the BN monolayer as well as the unintentional n-doping of $MoSe_2$. Additionally, a contribution from the misoriented domains and grain boundaries may also be present distorting the apparent band structure and work function.

To further support our argument that no new hybridization of bands takes place in $MoSe_2$/h-BN heterostructures, we have additionally performed vdW-DFT calculations.[39,40] The vertical heterostructure was modeled considering a (3 × 3) $MoSe_2$ supercell (a_{MoSe_2} ≈ 3.3 Å) on top of a (4 × 4) h-BN supercell ($a_{h\text{-}BN}$ ≈ 2.5 Å), as sketched in Figure 5a. Our simulations suggest that ML $MoSe_2$ is located ∼3.6 Å above the h-BN plane, with an interlayer interaction of ∼90 meV per f.u. and an adhesive energy of ∼9 meV/Å^2 per f.u. (Supporting Information Table 1). This latter value is below the typical adhesive energy of vdW-layered materials, estimated to be in the range of 13−21 meV/Å^2, thereby indicating a very weak coupling between the two layers in the heterostructure.[41] Figure 5b shows the charge transfer that takes place in the heterostructure: negative charge density distributes on both h-BN and $MoSe_2$ MLs, whereas positive charge accumulates in the interlayer region. Furthermore, the results of our vdW-DFT calculations presented in Figure 5c suggest that, in the heterostructure, the h-BN electronic states exist only below the energy of 0.7 eV below the VBM, as indicated by the dashed line. Therefore, $MoSe_2$ band edges are retained upon heterostructure formation, and the ML feature such as the direct band gap is thus preserved (Supporting Information Figures 8 and 9).

It is not clear why the nanomesh structure disappears with the deposition of $MoSe_2$, resulting in an atomically flat interface. The decoupling of h-BN from Rh occurs early in the MBE growth process as described in the Supporting Information section 5. This was not the case for the $MoSe_2$/h-BN/Ru system deposited by MBE,[15] where the nanomesh structure is unchanged even after the growth, and the electronic properties of $MoSe_2$ are modulated by the morphological variations due to the strong interaction with Ru. A similar disappearance of the nanomesh structure as in our case was observed for the graphene/h-BN/Rh(111)

DOI: 10.1021/acsnano.8b05628
ACS Nano XXXX, XXX, XXX−XXX

system, where the decoupling was assisted by the interfacial carbon formation between BN and Rh during the CVD growth of graphene. Here, we saw no evidence for the existence of the interfacial layer, and further investigation of the exact growth mechanism is required. Nevertheless, this route can be highly advantageous for utilizing technologically attractive qualities of the atomically flat, free-standing layers of $MoSe_2$ and other TMDs.

CONCLUSION

In conclusion, we demonstrate the growth of $MoSe_2$/h-BN heterostructures on Rh(111) with preferential lattice alignment *via* vdW epitaxy. The electronic properties of nominal ML $MoSe_2$/h-BN were directly revealed by *k*PEEM, showing the direct band gap with the VBM located at the *K* point and 0.23 eV above the Γ point. Additionally, the as-grown $MoSe_2$ was found to be virtually free-standing as the nanomesh h-BN structure becomes atomically flat during the growth. Photoluminescence from monolayer $MoSe_2$/h-BN can be detected after delaminating the heterostructure from the Rh substrate, and the electronic structure of the as-grown $MoSe_2$ remains preserved in the presence of the underlying h-BN, as confirmed by first-principles calculations. This work provides deep insights into the growth of TMDs on h-BN with highly attractive optoelectronic properties of pristine monolayer semiconductors.

METHODS

Material Growth. The growth was carried out in an Omicron MBE with $\sim 10^{-10}$ mbar base pressure. 1×1 cm^2 h-BN/Rh(111)/YSZ/Si(111) substrates were outgassed at up to 500 °C for 12 h prior to growth. The growth was conducted at 350 °C with a fixed Se/Mo ratio of ∼40 and a Mo deposition rate of ∼0.1 Å/min; the temperature was monitored using a pyrometer, and the flux for each cell was calibrated using a quartz crystal microbalance. After growth, the sample was postannealed *in situ* at the same temperature with Se flux at 400 °C for 20 min. A RHEED camera (STAIB Co.) was used to monitor the growth *in situ*. The LEED and photoelectron diffraction experiments were performed in the surface science laboratory at the University of Zurich.[42]

XPS and Raman Spectra and PL Characterizations. The XPS spectra were obtained *ex situ* in a commercial ULVC-PHI Versa Probe II system with a laboratory Al Kα X-ray source ($h\nu$ = 1486.6 eV), and the C 1s core-level peak at 284.8 eV was used as the reference for determining the binding energies. Peak identification and fitting was processed in PHI's MultiPak processing software. The PL and Raman spectra were measured using a 532 nm wavelength laser in a Renishaw Raman confocal microscope.

Photoemission Electron Momentum Microscopy. The experimental details of the instrument and *k*PEEM measurements can be found in previous reports.[33,34] In short, a *NanoESCA* MkI spectromicroscope (ScientaOmicron) equipped with a helium cold cathode lamp ($h\nu$ = 21.2 eV) was used for room-temperature *k*PEEM analysis in UHV conditions (2×10^{-10} mbar). The analyzer pass energy of 100 and 50 eV with an entrance slit size of 1 mm provided an energy resolution of 200 and 100 meV, respectively.

First-Principles Simulations. Our calculations were performed within the DFT framework, as implemented in the SIESTA code. In order to describe the exchange and correlation effects, we used the generalized gradient approximations of Perdew, Burke, and Ernzerhof (PBE) for free-standing $MoSe_2$ and several vdW density functionals (BH, C09, DRSLL, KBM, LMKLL) for the $MoSe_2$/h-BN heterostructure. Spin−orbit coupling was included only in the calculation of the band structure of free-standing $MoSe_2$. Core electrons were replaced with relativistic, Troullier−Martins pseudopotentials, whereas valence electrons were described with a Tζ *plus* double polarization (TZDP) basis set in conjunction with a mesh cutoff of 450 Ry. The basis set superposition error was systematically corrected following the counterpoise scheme. The Brillouin zone was sampled with the equivalent of $30 \times 30 \times 1$ *k*-points per $MoSe_2$ unit cell during geometry relaxation runs and $120 \times 120 \times 1$ *k*-points for the calculations of the electronic density of states. Tolerance on forces during relaxations was set to 15 meV/Å; lattice constants were set to be equal to that of the ML $MoSe_2$, and a 29 Å thick vacuum region was included to separate periodic replicas.

ASSOCIATED CONTENT

Supporting Information

The Supporting Information is available free of charge on the ACS Publications website at DOI: 10.1021/acsnano.8b05628.

Additional experimental details, supporting figures and table as described in text (PDF)

AUTHOR INFORMATION

Corresponding Author

*E-mail: andras.kis@epfl.ch.

ORCID

Jose Ignacio Pascual: 0000-0002-7152-4747
Thomas Greber: 0000-0002-5234-1937
Andras Kis: 0000-0002-3426-7702

Notes

The authors declare no competing financial interest.

ACKNOWLEDGMENTS

We thank M. Cantoni and D. Alexander (CIME) for FIB operation and for support with electron microscopy. We thank P. Mettraux for assistance with the XPS setup and experiments. The momentum microscopy was performed in the Platform for NanoCharacterization (PFNC) of MINATEC Campus within CEA-Grenoble research center. The access was provided by the NFFA-Europe Infrastructure (proposal ID 121) under Horizon 2020 EU Funding Program. We thank N. Gambacorti for coordinating the access to the NFFA-EU program. This work was financially supported by the European Research Council (Grant No. 240076) and has received funding from the European Union's Horizon 2020 research and innovation programme under Grant Agreement Nos. 696656 and 785219 (Graphene Flagship Core 1 and Core 2). M.P. acknowledges support by the Swiss National Science Foundation (Grant No. 200021-162612). First-principles calculations were performed at the Swiss National Supercomputing Centre (CSCS) under the project s832.

REFERENCES

(1) Radisavljevic, B.; Radenovic, A.; Brivio, J.; Giacometti, V.; Kis, A. Single-Layer MoS_2 Transistors. *Nat. Nanotechnol.* **2011**, *6*, 147−150.

(2) Splendiani, A.; Sun, L.; Zhang, Y.; Li, T.; Kim, J.; Chim, C.-Y.; Galli, G.; Wang, F. Emerging Photoluminescence in Monolayer MoS_2. *Nano Lett.* **2010**, *10*, 1271−1275.

(3) Mak, K. F.; Lee, C.; Hone, J.; Shan, J.; Heinz, T. F. Atomically Thin MoS_2: A New Direct-Gap Semiconductor. *Phys. Rev. Lett.* **2010**, *105*, 136805.

(4) Wang, Q. H.; Kalantar-Zadeh, K.; Kis, A.; Coleman, J. N.; Strano, M. S. Electronics and Optoelectronics of Two-Dimensional Transition Metal Dichalcogenides. *Nat. Nanotechnol.* **2012**, *7*, 699−712.

(5) Manzeli, S.; Ovchinnikov, D.; Pasquier, D.; Yazyev, O. V.; Kis, A. 2D Transition Metal Dichalcogenides. *Nat. Rev. Mater.* **2017**, *2*, 17033.

(6) Koma, A. Van Der Waals Epitaxy - a New Epitaxial-Growth Method for a Highly Lattice-Mismatched System. *Thin Solid Films* **1992**, *216*, 72−76.
(7) Dean, C. R.; Young, A. F.; Meric, I.; Lee, C.; Wang, L.; Sorgenfrei, S.; Watanabe, K.; Taniguchi, T.; Kim, P.; Shepard, K. L.; Hone, J. Boron Nitride Substrates for High-Quality Graphene Electronics. *Nat. Nanotechnol.* **2010**, *5*, 722−726.
(8) Yang, W.; Chen, G.; Shi, Z.; Liu, C.-C.; Zhang, L.; Xie, G.; Cheng, M.; Wang, D.; Yang, R.; Shi, D.; Watanabe, K.; Taniguchi, T.; Yao, Y.; Zhang, Y.; Zhang, G. Epitaxial Growth of Single-Domain Graphene on Hexagonal Boron Nitride. *Nat. Mater.* **2013**, *12*, 792−797.
(9) Britnell, L.; Gorbachev, R. V.; Jalil, R.; Belle, B. D.; Schedin, F.; Katsnelson, M. I.; Eaves, L.; Morozov, S. V.; Mayorov, A. S.; Peres, N. M. R.; Castro Neto, A. H.; Leist, J.; Geim, A. K.; Ponomarenko, L. A.; Novoselov, K. S. Electron Tunneling through Ultrathin Boron Nitride Crystalline Barriers. *Nano Lett.* **2012**, *12*, 1707−1710.
(10) Chhowalla, M.; Shin, H. S.; Eda, G.; Li, L.-J.; Loh, K. P.; Zhang, H. The Chemistry of Two-Dimensional Layered Transition Metal Dichalcogenide Nanosheets. *Nat. Chem.* **2013**, *5*, 263−275.
(11) Dumcenco, D.; Ovchinnikov, D.; Marinov, K.; Lazić, P.; Gibertini, M.; Marzari, N.; Sanchez, O. L.; Kung, Y.-C.; Krasnozhon, D.; Chen, M.-W.; Bertolazzi, S.; Gillet, P.; Fontcuberta i Morral, A.; Radenovic, A.; Kis, A. Large-Area Epitaxial Monolayer MoS_2. *ACS Nano* **2015**, *9*, 4611−4620.
(12) Fu, L.; Sun, Y.; Wu, N.; Mendes, R. G.; Chen, L.; Xu, Z.; Zhang, T.; Rümmeli, M. H.; Rellinghaus, B.; Pohl, D.; Zhuang, L.; Fu, L. Direct Growth of MoS_2/h-BN Heterostructures *via* a Sulfide-Resistant Alloy. *ACS Nano* **2016**, *10*, 2063.
(13) Wang, S.; Wang, X.; Warner, J. H. All Chemical Vapor Deposition Growth of MoS_2:H-BN Vertical van Der Waals Heterostructures. *ACS Nano* **2015**, *9*, 5246−5254.
(14) Vishwanath, S.; Liu, X.; Rouvimov, S.; Mende, P. C.; Azcatl, A.; McDonnell, S.; Wallace, R. M.; Feenstra, R. M.; Furdyna, J. K.; Jena, D.; Grace Xing, H. Comprehensive Structural and Optical Characterization of MBE Grown $MoSe_2$ on Graphite, CaF_2 and Graphene. *2D Mater.* **2015**, *2*, 024007.
(15) Zhang, Q.; Chen, Y.; Zhang, C.; Pan, C.-R.; Chou, M.-Y.; Zeng, C.; Shih, C.-K. Bandgap Renormalization and Work Function Tuning in $MoSe_2$/HBN/Ru(0001) Heterostructures. *Nat. Commun.* **2016**, *7*, 13843.
(16) Chen, M.-W.; Ovchinnikov, D.; Lazar, S.; Pizzochero, M.; Whitwick, M. B.; Surrente, A.; Baranowski, M.; Sanchez, O. L.; Gillet, P.; Plochocka, P.; Yazyev, O. V.; Kis, A. Highly Oriented Atomically Thin Ambipolar $MoSe_2$ Grown by Molecular Beam Epitaxy. *ACS Nano* **2017**, *11*, 6355.
(17) Chen, M.-W.; Kim, H.; Ovchinnikov, D.; Kuc, A.; Heine, T.; Renault, O.; Kis, A. Large-Grain MBE-Grown GaSe on GaAs with a Mexican Hat-like Valence Band Dispersion. *npj 2D Mater. Appl.* **2018**, *2*, 0047.
(18) Corso, M.; Auwärter, W.; Muntwiler, M.; Tamai, A.; Greber, T.; Osterwalder, J. Boron Nitride Nanomesh. *Science* **2004**, *303*, 217−220.
(19) Hemmi, A.; Bernard, C.; Cun, H.; Roth, S.; Klöckner, M.; Kälin, T.; Weinl, M.; Gsell, S.; Schreck, M.; Osterwalder, J.; Greber, T. High Quality Single Atomic Layer Deposition of Hexagonal Boron Nitride on Single Crystalline Rh(111) Four-Inch Wafers. *Rev. Sci. Instrum.* **2014**, *85*, 035101.
(20) Roth, S.; Matsui, F.; Greber, T.; Osterwalder, J. Chemical Vapor Deposition and Characterization of Aligned and Incommensurate Graphene/Hexagonal Boron Nitride Heterostack on Cu(111). *Nano Lett.* **2013**, *13*, 2668−2675.
(21) Xenogiannopoulou, E.; Tsipas, P.; Aretouli, K. E.; Tsoutsou, D.; Giamini, S. A.; Bazioti, C.; Dimitrakopulos, G. P.; Komninou, P.; Brems, S.; Huyghebaert, C.; Radu, I. P.; Dimoulas, A. High-Quality, Large-Area $MoSe_2$ and $MoSe_2/Bi_2$ Se_3 Heterostructures on AlN(0001)/Si(111) Substrates by Molecular Beam Epitaxy. *Nanoscale* **2015**, *7*, 7896−7905.
(22) Jiao, L.; Liu, H. J.; Chen, J. L.; Yi, Y.; Chen, W. G.; Cai, Y.; Wang, J. N.; Dai, X. Q.; Wang, N.; Ho, W. K.; Xie, M. H. Molecular-Beam Epitaxy of Monolayer $MoSe_2$: Growth Characteristics and Domain Boundary Formation. *New J. Phys.* **2015**, *17*, 053023.
(23) Wang, Y.; Zheng, Y.; Xu, X.; Dubuisson, E.; Bao, Q.; Lu, J.; Loh, K. P. Electrochemical Delamination of CVD-Grown Graphene Film: Toward the Recyclable Use of Copper Catalyst. *ACS Nano* **2011**, *5*, 9927−9933.
(24) Gao, L.; Ren, W.; Xu, H.; Jin, L.; Wang, Z.; Ma, T.; Ma, L.-P.; Zhang, Z.; Fu, Q.; Peng, L.-M.; Bao, X.; Cheng, H.-M. Repeated Growth and Bubbling Transfer of Graphene with Millimetre-Size Single-Crystal Grains Using Platinum. *Nat. Commun.* **2012**, *3*, 699.
(25) Kim, G.; Jang, A.-R.; Jeong, H. Y.; Lee, Z.; Kang, D. J.; Shin, H. S. Growth of High-Crystalline, Single-Layer Hexagonal Boron Nitride on Recyclable Platinum Foil. *Nano Lett.* **2013**, *13*, 1834−1839.
(26) Wen, Y.; Shang, X.; Dong, J.; Xu, K.; He, J.; Jiang, C. Ultraclean and Large-Area Monolayer Hexagonal Boron Nitride on Cu Foil Using Chemical Vapor Deposition. *Nanotechnology* **2015**, *26*, 275601.
(27) Caneva, S.; Weatherup, R. S.; Bayer, B. C.; Blume, R.; Cabrero-Vilatela, A.; Braeuninger-Weimer, P.; Martin, M.-B.; Wang, R.; Baehtz, C.; Schloegl, R.; Meyer, J. C.; Hofmann, S. Controlling Catalyst Bulk Reservoir Effects for Monolayer Hexagonal Boron Nitride CVD. *Nano Lett.* **2016**, *16*, 1250−1261.
(28) Cun, H.; Hemmi, A.; Miniussi, E.; Bernard, C.; Probst, B.; Liu, K.; Alexander, D. T. L.; Kleibert, A.; Mette, G.; Weinl, M.; Schreck, M.; Osterwalder, J.; Radenovic, A.; Greber, T. Centimeter-Sized Single-Orientation Monolayer Hexagonal Boron Nitride With or Without Nanovoids. *Nano Lett.* **2018**, *18*, 1205.
(29) Tongay, S.; Suh, J.; Ataca, C.; Fan, W.; Luce, A.; Kang, J. S.; Liu, J.; Ko, C.; Raghunathanan, R.; Zhou, J.; Ogletree, F.; Li, J.; Grossman, J. C.; Wu, J. Defects Activated Photoluminescence in Two-Dimensional Semiconductors: Interplay between Bound, Charged, and Free Excitons. *Sci. Rep.* **2013**, *3*, 2657.
(30) Tonndorf, P.; Schmidt, R.; Böttger, P.; Zhang, X.; Börner, J.; Liebig, A.; Albrecht, M.; Kloc, C.; Gordan, O.; Zahn, D. R. T.; Michaelis de Vasconcellos, S.; Bratschitsch, R. Photoluminescence Emission and Raman Response of Monolayer MoS_2, $MoSe_2$, and WSe_2. *Opt. Express* **2013**, *21*, 4908−4916.
(31) Zhang, Y.; Chang, T.-R.; Zhou, B.; Cui, Y.-T.; Yan, H.; Liu, Z.; Schmitt, F.; Lee, J.; Moore, R.; Chen, Y.; Lin, H.; Jeng, H.-T.; Mo, S.-K.; Hussain, Z.; Bansil, A.; Shen, Z.-X. Direct Observation of the Transition from Indirect to Direct Bandgap in Atomically Thin Epitaxial $MoSe_2$. *Nat. Nanotechnol.* **2013**, *9*, 111−115.
(32) Ross, J. S.; Wu, S.; Yu, H.; Ghimire, N. J.; Jones, A. M.; Aivazian, G.; Yan, J.; Mandrus, D. G.; Xiao, D.; Yao, W.; Xu, X. Electrical Control of Neutral and Charged Excitons in a Monolayer Semiconductor. *Nat. Commun.* **2013**, *4*, 1474.
(33) Frégnaux, M.; Kim, H.; Rouchon, D.; Derycke, V.; Bleuse, J.; Voiry, D.; Chhowalla, M.; Renault, O. Chemistry and Electronics of Single Layer MoS_2 Domains from Photoelectron Spectromicroscopy Using Laboratory Excitation Sources. *Surf. Interface Anal.* **2016**, *48*, 465−469.
(34) Kim, H.; Dumcenco, D.; Frégnaux, M.; Benayad, A.; Chen, M.-W.; Kung, Y.-C.; Kis, A.; Renault, O. Free-Standing Electronic Character of Monolayer MoS_2 in van Der Waals Epitaxy. *Phys. Rev. B: Condens. Matter Mater. Phys.* **2016**, *94*, 081401.
(35) Diaz, H. C.; Ma, Y.; Kolekar, S.; Avila, J.; Chen, C.; Asensio, M. C.; Batzill, M. Substrate Dependent Electronic Structure Variations of van Der Waals Heterostructures of $MoSe_2$ or MoSe $_{2(1-x)}Te_{2x}$ Grown by van Der Waals Epitaxy. *2D Mater.* **2017**, *4*, 025094.
(36) Jin, W.; Yeh, P.-C.; Zaki, N.; Zhang, D.; Sadowski, J. T.; Al-Mahboob, A.; van der Zande, A. M.; Chenet, D. A.; Dadap, J. I.; Herman, I. P.; Sutter, P.; Hone, J.; Osgood, R. M. Direct Measurement of the Thickness-Dependent Electronic Band Structure of MoS_2 Using Angle-Resolved Photoemission Spectroscopy. *Phys. Rev. Lett.* **2013**, *111*, 106801.
(37) Roth, S.; Greber, T.; Osterwalder, J. Some Like It Flat: Decoupled h-BN Monolayer Substrates for Aligned Graphene Growth. *ACS Nano* **2016**, *10*, 11187−11195.

DOI: 10.1021/acsnano.8b05628
ACS Nano XXXX, XXX, XXX−XXX

(38) Jin, W.; Yeh, P.-C.; Zaki, N.; Chenet, D.; Arefe, G.; Hao, Y.; Sala, A.; Mentes, T. O.; Dadap, J. I.; Locatelli, A.; Hone, J.; Osgood, R. M. Tuning the Electronic Structure of Monolayer Graphene/MoS_2 van Der Waals Heterostructures *via* Interlayer Twist. *Phys. Rev. B: Condens. Matter Mater. Phys.* **2015**, *92*, 201409.
(39) Soler, J. M.; Artacho, E.; Gale, J. D.; García, A.; Junquera, J.; Ordejón, P.; Sánchez-Portal, D. The SIESTA Method for *Ab Initio* Order- N Materials Simulation. *J. Phys.: Condens. Matter* **2002**, *14*, 2745.
(40) Berland, K.; Cooper, V. R.; Lee, K.; Schröder, E.; Thonhauser, T.; Hyldgaard, P.; Lundqvist, B. I. Van Der Waals Forces in Density Functional Theory: A Review of the VdW-DF Method. *Rep. Prog. Phys.* **2015**, *78*, 066501.
(41) Björkman, T.; Gulans, A.; Krasheninnikov, A. V.; Nieminen, R. M. Van Der Waals Bonding in Layered Compounds from Advanced Density-Functional First-Principles Calculations. *Phys. Rev. Lett.* **2012**, *108*, 235502.
(42) Greber, T; Raetzo, O.; Kreutz, T. J.; Schwaller, P.; Deichmann, W.; Wetli, E.; Osterwalder, J. A Photoelectron Spectrometer for *k*-Space Mapping above the Fermi Level. *Rev. Sci. Instrum.* **1997**, *68*, 4549.

DOI: 10.1021/acsnano.8b05628
ACS Nano XXXX, XXX, XXX−XXX